Seamless Control of Full-Bridge and Half-Bridge Topology Morphing *LLC* Converter Based on State Plane Analysis

Jie Chen, *Student Member, IEEE*, Junzhong Xu, *Member, IEEE*, and Yong Wang, *Member, IEEE*

***Abstract*—The topology morphing (TPM) strategy, which involves switching between full-bridge and half-bridge modes, offers a promising solution to broaden the voltage gain range of *LLC* converters without adding an extra device. However, due to the distinct voltage gain curves of these two modes, the existence of a stable operating point after TPM is not promised, resulting in system instability. To address this issue, this article proposes a design procedure based on peak gain trajectory, incorporating geometrically simplified steady-state state plane analysis. In this way, the predicted result shows a great agreement with the exact peak gain trajectory. In addition, a state plane–based topology morphing control (SPTMC) is introduced to mitigate significant output voltage transients caused by the abrupt TPM. With such a strategy, the desired switching frequency after TPM is forecasted and feedforward to the conventional linear control to ensure tight regulation of the output voltage during TPM. It is noted that neither a lookup table nor control scheme switching is required for the proposed control strategy. A prototype has been constructed to validate the feasibility of the proposed design procedure and the proposed SPTMC.**

***Index Terms*—Dynamic response, *LLC* converter, state plane analysis (SPA), topology morphing (TPM), wide gain.**

I. Introduction

THE *LLC* resonant converter has become popular over the past decade due to its advantageous features, such as high efficiency, easy implementation of zero voltage switching (ZVS), and hold-up capability [1], [2], [3]. However, certain applications requiring a wide voltage gain range can pose challenges in *LLC* converter design [4], [5], [6]. For example, in electric vehicle charging applications, to adapt to the mainstream automotive power battery voltage platforms, the output voltage range of the poststage dc–dc converter is required to be 200–1000 V, which is challenging for a standalone *LLC* converter to achieve such a wide gain range while maintaining high efficiency. One common solution involves employing a group of modularized *LLC* converter converters that can switch between series and parallel modes using relays [7], [8]. This approach, however, introduces high-voltage dc relays, increasing system cost and bulkiness. Thus, it is advantageous to explore alternative solutions that can improve the *LLC* converter voltage gain range without the need for additional circuits.

There are two common approaches to extend the voltage gain range of an *LLC* converter voltage gain range. The first approach involves adopting hybrid modulation, such as phase shift, pulsewidth modulation (PWM), or other new modulation schemes. These techniques provide the *LLC* converter modulation with a higher degree of freedom [9], [10], [11], [12]. However, implementing these new modulation schemes often requires topology modifications, which complicates the design and optimization, i.e., the ZVS range and optimized inductor RMS current should be reconsidered.

The second approach is known as topology morphing (TPM) [13], [14], [15], [16]. In this approach, the voltage gain of the full-bridge (FB) *LLC* converter is twice that of the half-bridge (HB) *LLC* converter at the same operating point. Based on such a concept, a switching strategy was proposed in [14] that allows the *LLC* converter to switch between FB and HB modes. Therein, FB mode is used to achieve high voltage gain as shown in Fig. 1(a), whereas the HB mode is employed in low gain situations as shown in Fig. 1(b). On this basis, a three-operation mode *LLC* converter was proposed in [15]. In addition to HB and FB modes, the *LLC* converter can also operate in a dual hybrid FB and HB mode by adding an additional leg on the primary side, which offers a voltage gain range between HB and FB modes. Another variation, presented in [16], introduces a series of HB (SHB), i.e., similar to a three-level *LLC* converter, and conventional HB modes in the *LLC* converter to further widen the gain range.

However, TPM does indeed face certain challenges. One of the issues, which is seldom studied in the literature, is the lack of stable operating points on the low gain curve after transitioning from a high gain mode to a low gain mode. Taking FB and HB morphing as an example, as shown in Fig. 1(c), the FB *LLC* converter reaches the frequency limit and performs TPM instruction at operation point I (OP_1). If the gain curve of HB mode is HB I, TPM can be completed successfully, and the *LLC* converter will operate at operation point II (OP_2) in HB mode. However, if the gain curve of the HB *LLC* converter is HB II, there is no operating point on the curve that matches the voltage

Manuscript received 28 March 2023; revised 5 July 2023; accepted 19 September 2023. Date of publication 26 September 2023; date of current version 6 December 2023. This work was supported by China Postdoctoral Science Foundation under Project 2022M722057. Recommended for publication by Associate Editor Q. Li. *(Corresponding authors: Junzhong Xu; Yong Wang.)*

The authors are with the Department of Electrical Engineering, Shanghai Jiao Tong University, Shanghai 200240, China (e-mail: chenjie1026@sjtu.edu.cn; junzhongxu@sjtu.edu.cn; wangyong75@sjtu.edu.cn).

Color versions of one or more figures in this article are available at https://doi.org/10.1109/TPEL.2023.3319333.

Digital Object Identifier 10.1109/TPEL.2023.3319333

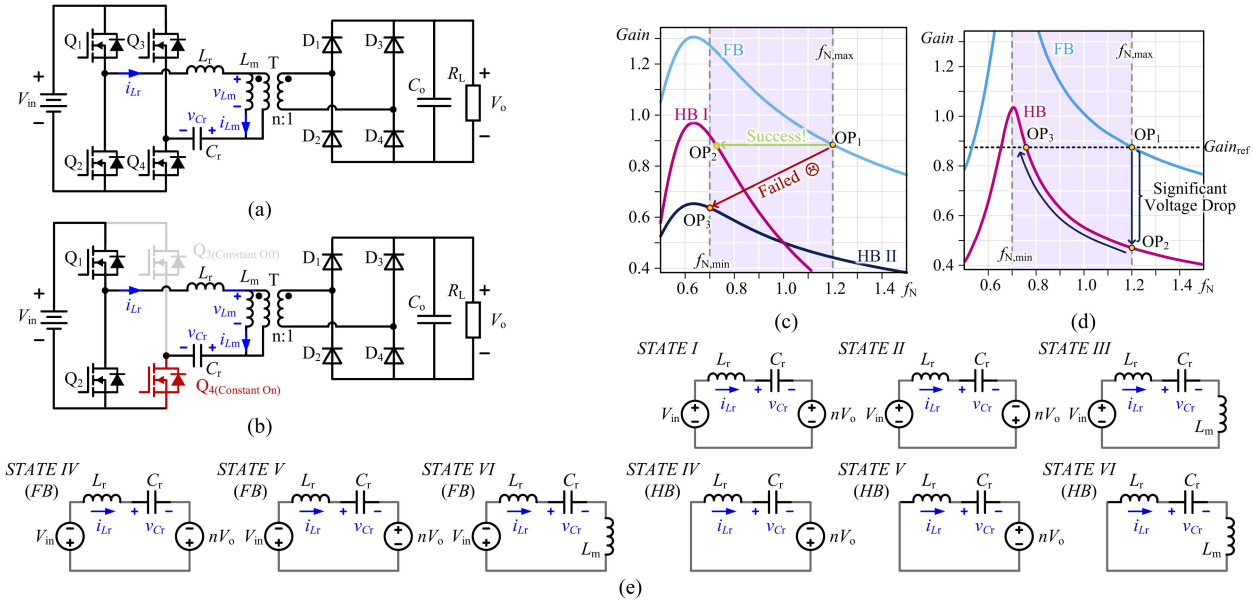

Fig. 1. (a) Topology of FB *LLC* converter. (b) Topology of HB *LLC* converter, where Q_4 (red) is constantly ON and Q_3 (gray) is constantly OFF. (c) TPM failure due to low voltage gain. (d) Significant voltage drop because of mismatching voltage gain. (e) Equivalent circuit of *LLC* converter under different state.

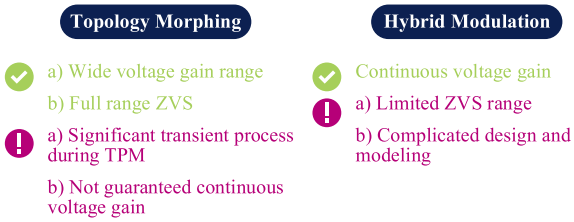

Fig. 2. Comparison between the hybrid modulation method and TPM method.

gain before TPM. While this issue can be addressed during the design procedure by considering the peak voltage gain curve into consideration conventional first harmonic approximation (FHA) analysis in boost mode is not accurate enough to serve as a reliable reference for *LLC* converter design [17], [18]. Therefore, it is necessary to explore precise methods for forecasting the gain.

Another challenge with the TPM approach is the occurrence of significant overshoot or undershoot during the transition, caused by the difference between the gain curves in different modes, as depicted in Fig. 1(d). To realize seamless TPM, the duty cycle of the morphing leg is gradually adjusted from 50% to nonswitching during the transition process [19]. However, this stepwise duty cycle variation consumes a significant amount of time. In [15], the switching frequency is fixed at a desired value during TPM to improve the dynamic performance. Yet, it requires the use of a lookup table, and all the data are collected through experiments, which can be time-consuming.

The comparison between the hybrid modulation method and the TPM method is depicted in Fig. 2. Although the TPM approach enjoys a wide voltage gain range with full range ZVS, the continuity of the voltage gain is seldom discussed and it suffers from the significant transient process during TPM.

To further improve the dynamic performance during TPM, state plane analysis (SPA) is introduced, where the resonant inductor current i_{Lr} and resonant capacitor voltage v_{Cr} are extracted to describe the transition of the resonant circuit in a 2-D state trajectory [20]. Through SPA, the optimal trajectory between two steady-state trajectories can be predicted, and optimal trajectory control (OTC) has been developed to achieve a fast dynamic response [21]. In [22] and [23], OTC is used to improve the dynamic performance during TPM between FB and HB *LLC* converters. In [24], OTC is adopted for the SHB mode *LLC* converter. Although OTC can achieve seamless TPM within a single switching cycle in theory, OTC have to be awakened as soon as possible to maintain its effectiveness in trajectory calculation, and thus a cycle-by-cycle control is indispensable, which is not friendly for a low-performance microcontroller unit (MCU). Moreover, the control scheme has to be switched between conventional linear control and OTC, i.e., transient control scheme switching is required, resulting in the increased likelihood of system instability [22].

In addition to the aforementioned transient state SPA, the steady-state SPA can predict the behavior of the resonant inductor current i_{Lr}, resonant capacitor voltage v_{Cr}, and dc gain characteristics at the specific operating points. However, these steady-state SPA models often involve high-order differential equations, making it challenging to obtain analytical solutions. Thus, simplification is expected to ease the complexity of the steady-state SPA. In this article, a design procedure based on geometrically simplified steady-state SPA is proposed for FB and HB morphing *LLC* converters and a corresponding seamless TPM control scheme is presented to solve the above issues of TPM *LLC*.

The contributions of this article are summarized as follows.

1) The peak voltage gain curve of *the LLC* converter is predicted through geometrically simplified SPA, which

can be used as an important criterion for *LLC* converter design. Besides, the expression of the desired switching frequency in boost mode is derived.

2) Based on the predicted *LLC* converter peak voltage gain curve, a design procedure for FB and HB morphing *LLC* converter was proposed. Herein, both the resonant capacitor voltage stress and the existence of a matching switching point are considered to ensure the stability of the converter.
3) A state plane–based topology morphing control (SPTMC) is proposed. The desired frequency variation is predicted online, and feedforward to the controller to optimize the dynamic performance during TPM.

The rest of this article is organized as follows. In Section II, the state plane of the *LLC* converter is introduced and a novel peak gain trajectory prediction method is proposed. Section III explains the procedure of the proposed FB and HB morphing *LLC* converter design. Section IV describes the principle of the proposed SPTMC. Section V gives the experiment results. Finally, Section VI concludes this article.

II. State Plane Analysis of Topology Morphing *LLC* Converter

A. *State Plane of* LLC *Converter*

The topology of the FB *LLC* converter is shown in Fig. 1(a). The resonant tank is composed of the resonant inductor L_r, the resonant capacitor C_r, and the magnetizing inductor L_m. The transformer ratio is n, and the input and output voltages are V_{in} and V_{out}, respectively. If Q_4 is constantly ON and Q_3 is constantly OFF as shown in Fig. 1(b), the topology morphs into an HB *LLC* converter. The gain of the HB *LLC* converter is half that of the FB *LLC* converter at the same operating point.

According to the conduction status of primary side switches and secondary side diode, the *LLC* converter can be separated into six different states in a single switching cycle, as shown in Fig. 1(e). Herein, FB and HB *LLC* converter share the same circuit in state I, II, and III, and differs in states IV, V, and VI. Both the ESR of all components and the diode forward voltage, which may slightly reduce the voltage, are ignored to simplify the analysis. With decent permutation and a combination of different states, *LLC* converters at various operating points can be obtained and studied. Through Kirchhoff's voltage laws, the normalized trajectories of all six modes are, respectively, written as follows [20]:

$$\begin{cases} (v_{CrN}-1+nV_{oN})^2+i_{LrN}^2=(V_{Cr0N}-1+nV_{oN})^2+I_{Lr0N}^2 \\ (v_{CrN}-1-nV_{oN})^2+i_{LrN}^2=(V_{Cr0N}-1-nV_{oN})^2+I_{Lr0N}^2 \\ (v_{CrN}-1)^2+Z_1^2 i_{LrN}^2/Z_0^2=(V_{Cr0N}-1)^2+Z_1^2 I_{Lr0N}^2/Z_0^2 \\ (v_{CrN}+a-nV_{oN})^2+i_{LrN}^2=(V_{Cr0N}+a-nV_{oN})^2+I_{Lr0N}^2 \\ (v_{CrN}+a+nV_{oN})^2+i_{LrN}^2=(V_{Cr0N}+a+nV_{oN})^2+I_{Lr0N}^2 \\ (v_{CrN}+a)^2+Z_1^2 i_{LrN}^2/Z_0^2=(V_{Cr0N}+a)^2+Z_1^2 I_{Lr0N}^2/Z_0^2 \end{cases} \tag{1}$$

where $Z_0=(L_r/C_r)^{1/2}$ and $Z_1=[(L_r+L_m)/C_r]^{1/2}$, v_{CrN} represents the normalized resonant capacitor voltage, i_{LrN} is the normalized resonant inductor current, V_{oN} denotes the normalized output voltage, and V_{cr0N} and I_{cr0N} are defined as the normalized initial condition under each state. a is 0 for HB mode and 1 for FB mode. All the variables are normalized as follows:

$$\begin{cases} f_N=f_s/f_r \\ v_N=v/V_{in} \\ i_N=i/(V_{in}/Z_0) \\ t_r=1/f_r \\ M=V_{in}/nV_o \end{cases} \tag{2}$$

where $f_r=\omega_r/2\pi$ is the resonant frequency, $\omega_r=(1/L_rC_r)^{1/2}$ is the resonant angular frequency, f_s is the switching frequency, t_r is the resonant cycle, and M refers to the voltage gain.

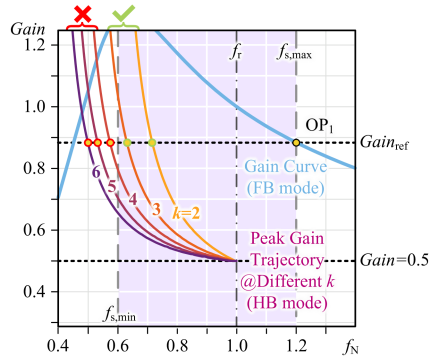

Fig. 3. Peak gain trajectory with different inductor ratio k after TPM (HB mode) and gain curve before TPM (FB mode), where the purple region illustrates the allowable switching frequency range and the red and green dots stand for the possible operating point after TPM.

B. *Peak Gain Prediction of* LLC *Converter With SPA*

Although the FB and HB morphing *LLC* converter features an extended voltage gain range, the converter system will become unstable, if there is no suitable HB mode operating point when the FB *LLC* converter performs the TPM instruction. The cause of the absence of a suitable operating point can be concluded as follows:

1) low voltage gain due to heavy load as shown in Fig. 1(c);
2) a wide switching frequency range is required because of the large inductor ratio k, as shown in Fig. 3.

As shown in Fig. 3, when the *LLC* converter switches from FB to HB at OP_1, stable operating points (with the same voltage gain TPM) definitely exist within the frequency limits, i.e., k is 2 or 3. It is because the inductive operating region is on the right side of the peak gain trajectory, and the minimum switching frequency to achieve a certain voltage gain can be considered as the frequency at which the peak gain trajectory reaches such voltage gain. Yet, the desired frequency to maintain the same voltage gain decreases, as the inductor ratio k increases, and thus the existence of a certain working point cannot be confirmed if k is greater than 4.

Therefore, one basic requirement to guarantee the accomplishment of TPM is that the peak gain at the minimum switching frequency of HB mode must be greater than the reference

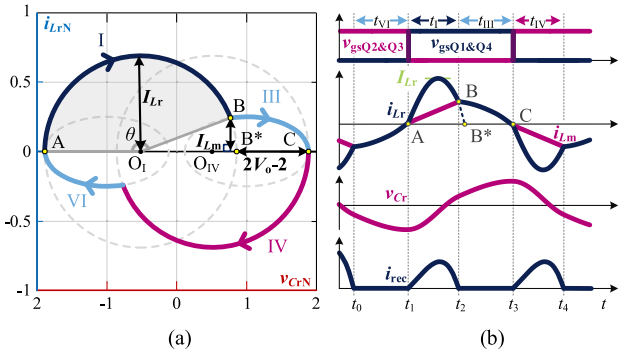

Fig. 4. (a) State plane (*x*-axis: normalized resonant capacitor voltage v_{CrN}, *y*-axis: normalized resonant inductor current i_{LrN}) and (b) key waveforms of *LLC* converter at the peak voltage gain.

voltage. In this section, the prediction of peak gain trajectory will be derived via geometrically simplified SPA.

It is noted that while the soft switch requires a certain amount of reverse current to be effective, the dead time effect has minimal impact on the peak gain curve, i.e., the ZVS/non-ZVS boundary deviates from the peak gain curve in practice. Therefore, in the derivation process, both dead time and parasitic parameters can be disregarded.

The peak gain trajectory is the boundary between the capacitive region and inductive region of the *LLC* converter, and also the dividing line whether the primary side MOSFET can implement ZVS. Fig. 4(b) shows the waveform of FB *LLC* converter at peak gain, where i_{LrN} is 0 and Q_1 and Q_4 are critically ZVS turned ON at A.

In Fig. 4(a), v_{CrN} and i_{LrN} are extracted, as the *x*-axis and *y*-axis, to plot the state plane trajectory. It can be seen that the *LLC* converter has four states (I, III, IV, and VI) at the peak gain. The only criterion for the converter to operate at the peak gain is that the starting points of both states I and IV are on the *x*-axis. Thus, the *LLC* converter peak gain trajectory can be obtained by calculating the gain and the time period required for the converter to run around such a trajectory that meets the criterion.

The switching cycle at peak gain t_{peak} can be decomposed into the duration of states I, III, IV, and VI, which are t_I, t_{III}, t_{IV}, and t_{VI}, respectively. Because the two half-cycles of the *LLC* converter are symmetric with each other, t_{peak} can be written as

$$t_{peak} = t_I + t_{III} + t_{IV} + t_{VI} = 2t_I + 2t_{III}. \tag{3}$$

In state III, the resonant capacitor C_r is charged from B to C, where B and C are the starting and ending points of state III, respectively. According to the ampere second principle, the voltage between B and C can be obtained as

$$\Delta v_{CrN\_BC} = \int_{t_2}^{t_2+t_{III}} \frac{i_{LrN}}{Z_0 C_r} dt \tag{4}$$

where i_{LrN} gradually decreases from the resonant inductor current at B (i_{LrN_B}) to 0. Taking the average of i_{LrN}, it can be regarded that C_r is charged by constant current i_{LrN_B} /2, and t_{III} can be written as

$$t_{III} = \frac{2\Delta v_{CrN\_BC} Z_0 C_r}{i_{LrN\_B}}. \tag{5}$$

Since B is the ending point of state I, the resonant inductor current i_{LrN_B} is equal to the magnetizing inductor current i_{LmN_B} at B. By assuming that the durations of t_1 to t_2 and t_2 to t_3 are the same as t_s/4, L_m is clamped at nV_{oN} from t_1 to t_2 for t_s/4. According to the volt-second principle, i_{LrN_B} can be calculated as

$$i_{LrN\_B} = i_{LmN\_B} = \int_0^{0.25t_s} \frac{nZ_0 V_{oN}}{L_m} dt = \frac{\pi n V_{oN}}{2k f_N} \tag{6}$$

where k is equal to L_m/L_r, i.e., the inductor ratio.

Because L_m is far greater than L_r, i_{LrN_B} is small compared with the radius of the state I trajectory. Point B is thus located close to B*, where B* is the intersection of state I and the *x*-axis, as shown in Fig. 4(b). Therefore, the resonant capacitor voltage difference between B and C (Δv_{CrN_BC}) can be simplified as that between point B* and C (Δv_{CrN_B*C}). As B*C is equal to the center distance between states I and IV, Δv_{CrN_B*C} can be obtained as

$$\Delta v_{CrN\_B*C} = 2nV_{oN} - 1 - a. \tag{7}$$

By taking (6) and (7) into (5), t_{III} can be derived as

$$t_{III} = \frac{4L_m f_N}{\pi Z_0}\left(2 - \frac{1+a}{nV_{oN}}\right). \tag{8}$$

In the state I, the resonant circuit runs from A to B, and t_I can be given as

$$t_I = \frac{\theta}{\omega_r} \tag{9}$$

where θ is the central angle of arc AB and can be calculated as

$$\theta = \arcsin \frac{i_{LrN\_B}}{I_{LrN}} \tag{10}$$

where I_{LrN} is the radius of state I trajectory, which can be further written as

$$I_{LrN} = v_{CrN\_B*} - 1 + nV_{oN} = v_{CrN\_C} + a - nV_{oN} \tag{11}$$

where v_{CrN_B*} and v_{CrN_C} are the resonant capacitor voltage at B* and C, respectively. The trajectory of state III can be converted into the time domain as

$$\begin{cases} i_{LrN} = I_{LrN\_III} \sin\left(\frac{\omega_r}{\sqrt{k+1}} t + \phi_0\right) \\ v_{CrN} = -\sqrt{k+1} I_{LrN\_III} \cos\left(\frac{\omega_r}{\sqrt{k+1}} t + \phi_0\right) + 1 \end{cases} \tag{12}$$

where I_{LrN_III} is the normalized amplitude of the inductor current in state III, and ϕ_0 is the initial phase of state III.

Since B is the starting point of state III, and C is the ending point of state III, i_{LrN_B} and v_{CrN_C} can be rewritten as

$$\begin{cases} i_{LrN\_B} = I_{LrN\_III} \sin\left(\pi - \frac{t_{III}\omega_r}{\sqrt{k+1}}\right) \\ v_{CrN\_C} = -\sqrt{k+1} I_{LrN\_III} \cos\pi + 1 \end{cases}. \tag{13}$$

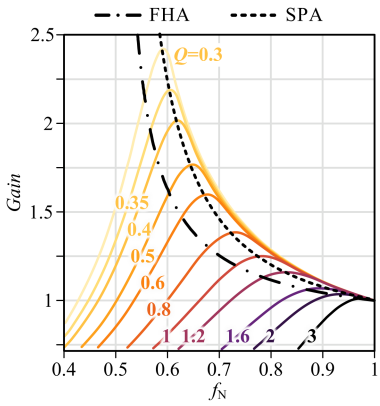

Fig. 5. Peak gain trajectory predicted by SPA and FHA, and the gain curve obtained via simulation.

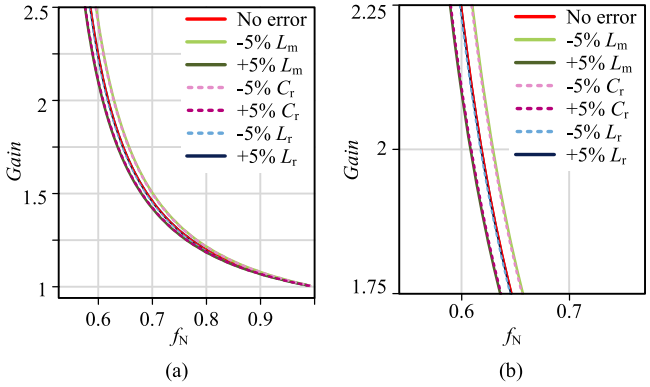

Fig. 6. (a) Impact of the resonant circuit parameter error on the peak gain curve. (b) Zoomed-in view.

By taking (6), (8), (10), (11), and (13) into (9), t_I can be given as

$$t_I = \frac{1}{\omega_r} \arcsin \frac{1}{\frac{\sqrt{k+1}}{\sin[\frac{4kf_N}{\pi\sqrt{k+1}}(2-\frac{1+a}{nV_{oN}})]} + \frac{2kf_N}{\pi}}. \tag{14}$$

It should be noted that (14) is the modified expression of t_I, and its procedure is explained in Appendix.

By substituting (8) and (14) into (3), the peak gain trajectory can be given as

$$f_{s\_peak} = \frac{1}{2t_I + 2t_{III}}. \tag{15}$$

The peak gain trajectory is shown in Fig. 5, where $Q = (L_r/C_r)^{1/2}/R_L$, i.e., the quality factor, and R_L is the equivalent resistance of the load. The peak gain trajectory predicted by SPA shows great accuracy, and the result obtained via FHA analysis is far from the actual curve.

The impact of parameter errors in the resonant circuit on the peak gain curve is shown in Fig. 6. It can be observed that when there is a variation in L_m, it affects the inductance ratio. A lower value of L_m will result in the operating point of the peak gain appearing at a higher switching frequency, and vice versa. As for the error of resonant capacitor C_r, only the resonant frequency shifts, leading to the overall translation of the peak gain curve. In the case of a change in L_r changes, there is a simultaneous alteration in both the inductance ratio and resonant frequency, forming a certain level of compensation, and the peak gain curve remains almost unchanged compared to the scenario without parameter errors.

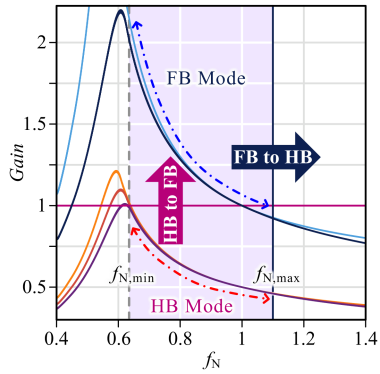

Fig. 7. Gain curve and TPM principle of FB and HB morphing *LLC* converter designed according to the principle proposed in this article.

III. Design of Topology Morphing *LLC* Converter

With the aforementioned peak voltage gain trajectory, the existence of a stable operating point after TPM can be guaranteed during the design process. In this section, a design procedure for FB and HB TPM *LLC* converter is proposed. Before the explanation of the detailed procedure, the TPM criterion and the morphing principle need to be explained for the aim of easy understanding.

A. Morphing Principle of the Proposed LLC Converter

Fig. 7 shows the gain curve of FB and HB morphing *LLC* converter designed according to the principle proposed in this article, where $f_{N,min}$ is the nominal minimum switching frequency of the *LLC* converter which is defined by the user based on the compromise of power density, efficiency, and electromagnetic interference performance. $f_{N,max}$ is the nominal maximum switching frequency and is slightly higher than the resonant frequency to maintain high efficiency, which in this article is $1.1f_r$.

If the switching frequency reaches $f_{N,max}$ in FB mode, the converter will receive the morphing instructions. In the HB mode, the converter will switch to FB mode if the gain is greater than the threshold gain M_{th}, which is set to 1 to ensure successful TPM to FB mode and allow margin in this article.

While it is possible to modify the threshold of the TPM in *LLC* converters operating in FB mode to optimize efficiency and allow them to operate in buck mode, this article primarily focuses on the continuity of voltage gain in the FB/HB mode due to space limitations. As a result, we only consider a specific case where the voltage gain threshold from HB to FB is set to 1, and there is no need to consider the frequency constraint of

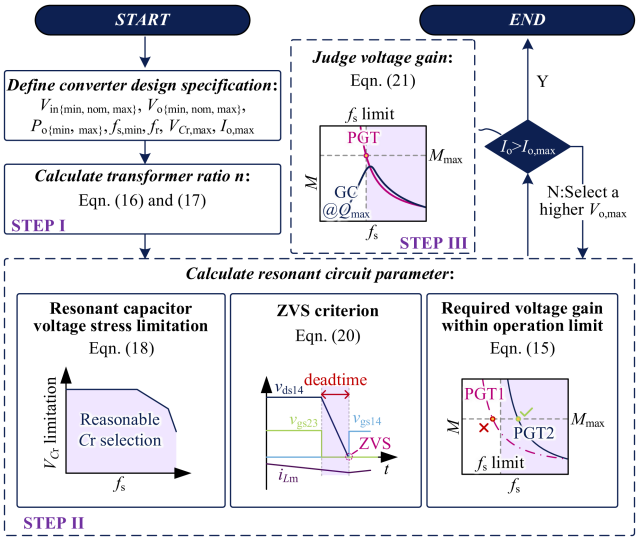

Fig. 8. Flowchart of the proposed design process of FB and HB morphing *LLC*, where PGT stands for peak gain trajectory and GC means the gain curve.

the light-load buck mode. Therefore, the analysis in this article solely focuses on the boost mode.

Since both the minimum switching frequency $f_{s,min}$ and the maximum resonant capacitor voltage stress $V_{Cr,max}$ occur at the operating point of maximum output power $P_{o,max}$ and maximum voltage gain [25], it is only necessary to focus on the operating point at $P_{o,max}$ and maximum voltage gain M_{max} in FB modes. For HB mode, the consideration is the same, whereas the maximum voltage gain M_{max} is replaced with morphing voltage gain threshold M_{th}.

B. *Design Procedure of Topology Morphing* LLC *Converter*

A novel design process of FB and HB morphing *LLC* converter is presented, whose flowchart is shown in Fig. 8. Each step and its principle are described as follows.

Step I: After obtaining the design specification, the transformer ratio of the converter is determined first. If there is a nominal output voltage $V_{o,nom}$ and $V_{o,nom}/V_{in,nom}<2V_{o,min}/V_{in,max}$, the transformer ratio can be written as

$$n = \frac{V_{o,nom}}{V_{in,nom}}. \tag{16}$$

Else, to cover the whole voltage gain range, the minimum voltage gain operating point is set as the resonant point of HB mode, and the transformer ratio is set as

$$n = \frac{2V_{o,min}}{V_{in,max}}. \tag{17}$$

Step II: As mentioned before, it is only necessary for the designed converter to be able to output sufficient voltage gain (M_{max} or M_{th}) and power ($P_{o,max}$) in both FB and HB modes while satisfying the resonant capacitor voltage stress ($V_{Cr,max}$) and switching frequency range ($f_{s,min}$).

1) Resonant Capacitor Voltage Stress: For the resonant capacitor, its voltage stress can be obtained as [2]

$$V_{Cr} = V_o - V_{in} + Z_r\sqrt{\left(\frac{I_o\pi}{2n}\right)^2 + \left(\frac{nV_o}{4L_m f_s}\right)^2}. \tag{18}$$

By taking the corresponding operating point into (18), $V_{Cr,max}$ in FB and HB modes can be, respectively, written as

$$\begin{cases} V_{Cr,max\_FB} = V_{o,max} - V_{in,min} \\ \qquad\qquad + Z_r\sqrt{\left(\frac{I_{o,max}\pi}{2n}\right)^2 + \left(\frac{nV_{o,max}}{4L_m f_{s,min}}\right)^2} \\ V_{Cr,max\_HB} = V_{o,nom} + Z_r\sqrt{\left(\frac{I_{o,max}\pi}{2n}\right)^2 + \left(\frac{nV_{o,nom}}{4L_m f_{s,min}}\right)^2} \end{cases}. \tag{19}$$

2) Peak Voltage Gain Curve: For *LLC* converter to achieve the operating point of $P_{o,max}$ and M_{max} within the switching frequency range and to ensure successful TPM from FB to HB, a sufficiently small inductor ratio k is required. It can be seen in Fig. 3 that if k is too large, the desired operating point of the certain gain may not be within the switching frequency range. However, a too small k can cause a large reactive current and thus lead to low efficiency.

To maintain high efficiency, the largest k is found by making the peak gain trajectory meet the required voltage gain (M_{max} in FB mode and M_{th} in HB mode) at $f_{s,min}$, and thus the operating point can be ensured to be within the switching frequency range. That is to take the corresponding operation point into (3).

3) ZVS Criterion: Furthermore, ZVS needs to be guaranteed, whose criterion is to finish the charging and discharging process of the MOSFET drain–source capacitance C_{ds} within the dead time t_d. To ensure that the *LLC* converter can achieve ZVS, the *LLC* converter needs to meet the following requirements [26]:

$$L_m < \frac{t_d}{16C_{ds}f_s}. \tag{20}$$

Combined with the definition of resonant frequency f_r, the resonant circuit parameters can be obtained by simultaneous equations (3), (18), and (20).

Step III: Nevertheless, peak gain is independent of load condition. The scenario that there is no certain operation point under such load may occur as shown in Fig. 1(c). Therefore, the output current I_o of the peak gain at the minimum switching frequency needs to be verified whether it is larger than the desired load. As I_o is the average of the current in the secondary side (i_{rec}), I_o can be written as

$$I_o = \frac{2}{t_s}\int_{t_1}^{t_2} I_{LrN}\frac{V_{in}}{Z_0}\sin\omega_r(t-t_1) - \frac{nV_o t}{L_m}dt. \tag{21}$$

If I_o is greater than the desired load, this set of parameters can be used. Otherwise, a higher V_o is defined and redo Step II.

In practice, as all the inductive operating points are on the right side of the peak gain trajectory as shown in Fig. 5, the *LLC* converter will not work exactly at the peak gain point if the resonant circuit parameter is qualified. Therefore, a margin of frequency is allowed.

TABLE I
CONVERTER DESIGN SPECIFICATION

Items	Designator	Min	Max
Input voltage	V_{in}	120 V (Nominal)	
Output voltage	V_o	50 V	200 V
Output power	P_o	300 W (Nominal)	
Switching frequency	f_s	100 kHz	–
Resonant frequency	f_r	150 kHz	–
Resonant capacitor voltage stress	V_{Cr}	–	700 V
Output current	I_{max}	–	3 A

TABLE II
CIRCUIT PARAMETER

Items	Value
Transformer ratio n	12:10
Resonant inductor L_r	14.3 μH
Magnetizing inductor L_m	40 μH
Resonant capacitor C_r	85 nF

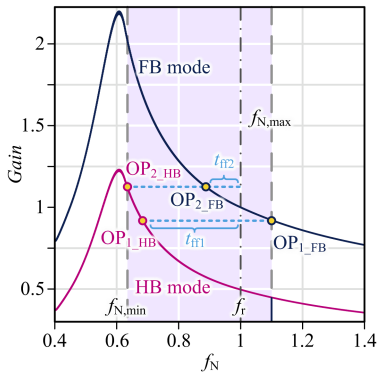

Fig. 9. Gain curve of the *LLC* converter with the TPM criterion of switching frequency.

The specifications of the *LLC* resonant converter are listed in Table I. The calculated component parameters of the illustrative example are summarized in Table II.

IV. STATE PLANE–BASED TOPOLOGY MORPHING CONTROL

To avoid significant output voltage transients and ensure tight regulation of output voltage during TPM, a novel SPTMC is proposed in this article. Different from the previous feedforward-based TPM control requiring a lookup table, the basic principle of the SPTMC is via predicting the desired switching frequency online after TPM and feedforwarding it to the linear controller.

In this section, the voltage gain in boost mode is discussed through geometrically simplified SPA at first, because the operating point of *LLC* converter after TPM is always in boost mode. Then, the detailed control strategy is described.

Fig. 9 shows the gain curve of the *LLC* converter with the TPM criterion of switching frequency. For FB to HB TPM, when the *LLC* converter reaches the maximum switching frequency limit at OP_{1_FB} in FB mode, it will switch to HB mode. The voltage gain at OP_{1_FB} is prevented from being designed lower than 0.5 for the consideration of efficiency. Thus, to maintain the same gain before and after TPM, the *LLC* converter will eventually

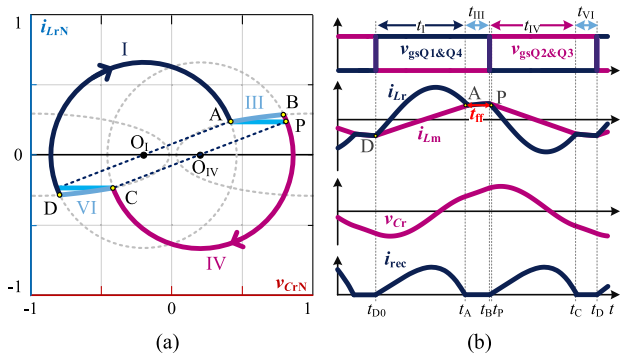

Fig. 10. (a) State plane of *LLC* converter in boost mode (*x*-axis: normalized resonant capacitor voltage v_{CrN}, *y*-axis: normalized resonant inductor current i_{LrN}). (b) Key waveform of *LLC* converter in boost mode.

work at OP_{1_HB}, which is boost mode for HB mode. When the *LLC* converter switches from HB to FB, to avoid an unstable operating point in light-load FB buck mode after TPM, OP_{2_FB} (switched from OP_{2_HB}) also should be designed to work in boost mode.

A. Boost Mode Voltage Gain Prediction of LLC Converter With SPA

Thus, to ensure that the *LLC* converter can quickly find the stable operating point after TPM to achieve a tight regulation of the output voltage, it is important to analyze the operation state and the desired switching frequency in boost mode.

To predict the desired switching frequency of the *LLC* converter after TPM, steady-state SPA is performed, as shown in Fig. 10. In boost mode, the *LLC* converter has four states (I, III, IV, and VI), and the switching cycle can be written as

$$t_s = t_I + t_{III} + t_{IV} + t_{VI} = 2t_I + 2t_{III}. \tag{22}$$

Because L_m is far greater than L_r, the resonant inductor current i_{LrN} can be assumed constant during states III and VI as shown in Fig. 10(b). Thus, i_{LrN} is opposite at A and D, where A and D are the ending and starting points of state I, respectively. The duration of mode I (t_I) can be obtained as $t_r/2$.

It can be seen in Fig. 10(a) that P is the ending point of mode III if i_{LrN} is constant in mode III. AP is parallel to the *x*-axis and thus can be considered as the change of v_{CrN} during state III. It can be derived that AP is equal to O_1O_2, where O_1 and O_2 are the centers of states I and IV trajectory. Thus, the normalized resonant capacitor voltage between A and P (v_{CrN_AP}) can be given as

$$v_{CrN\_AP} = AP = O_1O_2 = 2nV_{oN} - 1 - a. \tag{23}$$

As the resonant inductor current i_{LrN} is considered constant during state III, t_{III} can be accounted as the time for C_r to be charged with $2nV_{oN}$-1-a by a constant current i_{LrN_A}. As a result, t_{III} can be written as

$$t_{III} = \frac{2nV_{oN} - 1 - a}{i_{LrN\_A}} C_r \tag{24}$$

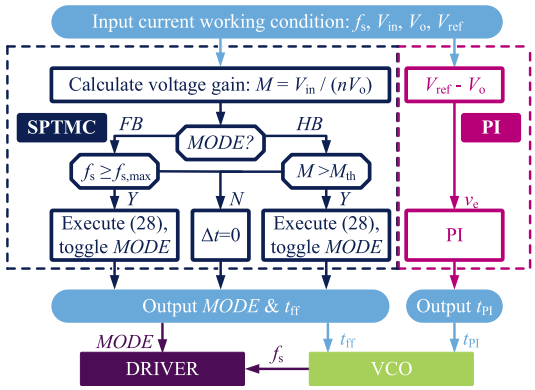

Fig. 11. Control block diagram of the proposed SPTMC.

where i_{LrN_A} is the resonant current at A. Since A is the beginning of mode III, i_{LrN_A} is equal to the magnetizing inductor current i_{LmN_A} at A. The magnetizing inductor voltage V_{LmN} is clamped at nV_{oN} in mode I for $t_r/2$, and $-nV_{oN}$ in mode IV for another $t_r/2$. According to the volt-second principle, i_{LrN_A} is thus obtained as

$$i_{LrN\_A} = i_{LmN\_A} = \frac{1}{2}\int_0^{0.5t_r} \frac{V_{LmN}}{L_m} dt = \frac{\pi n V_{oN}}{2k}. \quad (25)$$

By replacing V_o with V_{ref}, t_{III} in boost mode can be given as

$$t_{III} = \frac{v_{CrN\_AP}}{i_{LrN\_A}} C_r = \left(2 - \frac{1+a}{nV_{oN}}\right) \frac{2C_r k}{\pi}. \quad (26)$$

Thus, the relationship between the voltage gain and the switching frequency of the *LLC* converter under boost mode can be written as follows:

$$f_N = \frac{1}{1 + (2 - \frac{1+a}{nV_{oN}}) \frac{k}{2\pi^2 Z_0}}. \quad (27)$$

B. Detailed Control Scheme

With the switching frequency expression as (27), a novel SPTMC is proposed, whose control block diagram is shown in Fig. 11. In the steady state, the converter is under PI control. When TPM instruction is performed, the target *MODE* is determined by SPTMC and the desired switching frequency is feedforward.

To be specific, in SPTMC, *MODE* in operation is judged at first, and then the operation point is determined whether it exceeds the mode limit. If it does, TPM is required. *MODE* is toggled, and the feedforward frequency Δf is obtained. Else, Δf is set to 0. The feedforward frequency Δf is the difference between the desired frequency after TPM and the current switching frequency.

It should be noted that the mode limit is defined by the user. Either switching frequency, gain, or hybrid limitation can be selected. In the proposed design method, the criterion of HB to FB morphing is that the gain is greater than 1. Obviously, the desired frequency is the resonant frequency in this case. To make the proposed control universal, the feedforward frequency during HB to FB morphing with frequency criterion is also presented.

Through (27), the feedforward values during TPM can be written as

$$\begin{cases} \Delta f_s = \frac{1}{1+(2-\frac{1}{nV_{oN}})\frac{k}{2\pi^2 Z_0}} - f_{N,max}(\text{FB to HB}) \\ \Delta f_s = \frac{1}{1+(1-\frac{1}{nV_{oN}})\frac{k}{\pi^2 Z_0}} - f_{N,min}(\text{HB to FB}) \end{cases}. \quad (28)$$

C. Simulation Results

Simulation has been conducted to validate the feasibility of the proposed SPTMC and compare its performance with other methods discussed in previous papers. The specifications in the simulation are given in Table II, and the output capacitor C_o is 15 μF. The topology used in the simulation is identical to that shown in Fig. 1(a).

As shown in Fig. 12, the performance of the proposed SPTMC is compared with PI control, the method presented in [19], and SPTMC combined with OTC as described in [23]. The results reveal that under SPTMC, the output voltage overshoot is only 5% of that observed under PI control when the converter switches from HB to FB. Similarly, the overshoot is 10% when the converter switches from FB to HB. While the method presented in [19] shows lower overshoot (or undershoot) compared to SPTMC, its transient time is 12 times slower than that achieved by the proposed SPTMC method.

Due to the little energy stored in the resonant circuit, there is minimal impact on the dynamic performance of the *LLC* converter. As depicted in Fig. 12(e) and (f), both the settling time and the overshoot (or undershoot) of the SPTMC are almost the same as those achieved by combining OTC with SPTMC (OTC+SPTMC), implying that the main optimization effect of OTC, as presented in [23], relies on the feedforward mechanism of the desired switching frequency after TPM.

The main improvement of OTC is its ability to suppress the oscillation of the resonant circuit caused by TPM. It can be seen in Fig. 12(g) and (h) that the voltage overshoot (or undershoot) immediately after the TPM of OTC+SPTMC is significantly lower compared to that observed with SPTMC, as an extra (missing) conduction period is inserted through OTC.

Furthermore, through Fig. 12(e)–(h), it can be observed that due to that the energy stored in the resonant circuit has little impact on the output voltage, the *LLC* converters TPM using the proposed SPTMC can be considered as momentarily switching from one steady-state to another (of course, the operating point after switching may deviate slightly from the ideal operating point due to inaccurate feedforward). Therefore, the stability analysis only needs to be conducted on the two steady-state points before and after TPM. As long as the PI parameters are sensible and the voltage gain is continuous, the system is certain to be stable.

Fig. 13 shows the impact of resonant component tolerances on SPTMC. It is evident that the deviated resonant parameter may slightly degrade the performance. However, such a reduction in performance is acceptable, as the output voltage overshoot (or

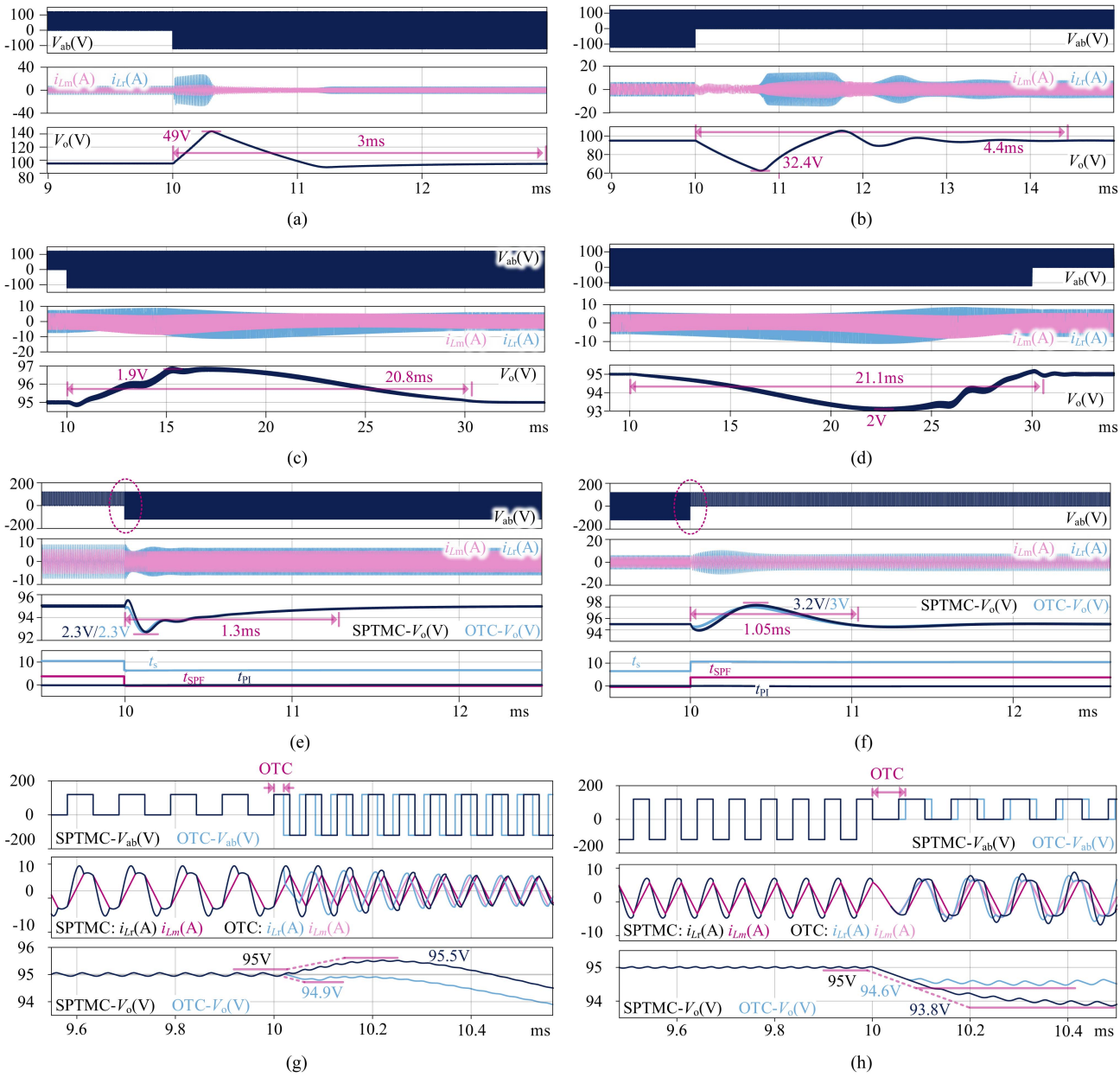

Fig. 12. Key waveform of TPM *LLC* converter switching between FB and HB modes under different controllers. PI controller only (a) from HB to FB and (b) from FB to HB. Strategy in [19](c) from HB to FB and (d) from FB to HB. The proposed SPTMC with and without OTC (e) from HB to FB and (f) from FB to HB. Enlarged view of the proposed SPTMC with and without OTC (g) from HB to FB and (h) from FB to HB.

undershoot) of the SPTMC with the deviated resonant parameter remains below 20% of that achieved with PI control alone.

V. Experiment Results

The prototype is shown in Fig. 14, whose topology is identical to that in Fig. 1(a). The specifications of the prototype are given in Table III.

A. Peak Gain Curve

As shown in Fig. 15, the peak gain trajectory predicted via geometrically simplified SPA enjoys good accuracy with the experiment results, when the quality factor Q is greater than 0.5.

B. Topology Morphing Dynamic Performance

Fig. 16 shows the key waveform of the TPM *LLC* converter switching between FB and HB modes under different controllers. It can be seen that if only the PI controller is adopted, tremendous output voltage transient happens during TPM, which can definitely damage the back-stage electrical equipment. The undershoot and overshoot of output voltage are improved with the controller in [19]. Yet, the morphing procedure is very long.

Fortunately, with the proposed SPTMC, the *LLC* converter can maintain tight regulation during TPM, and the transient process is shortened to within 2 ms in both HB to FB and

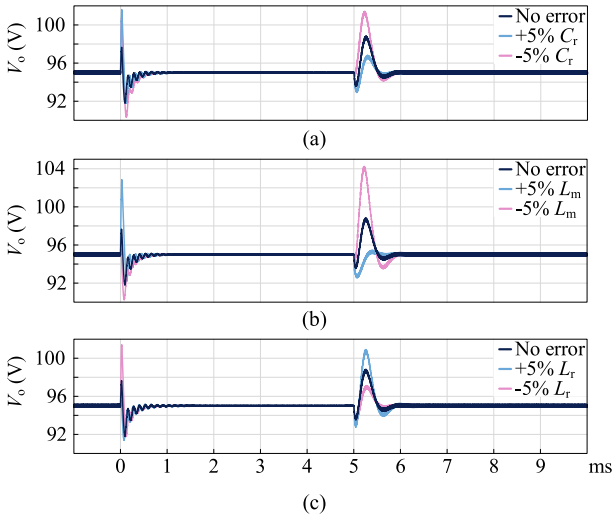

Fig. 13. Key waveform of TPM *LLC* converter switching between FB and HB modes with the proposed STMC under resonant component parameter offset. (a) +5% and -5% C_r. (b) +5% and -5% L_m. (a) +5% and -5% L_r.

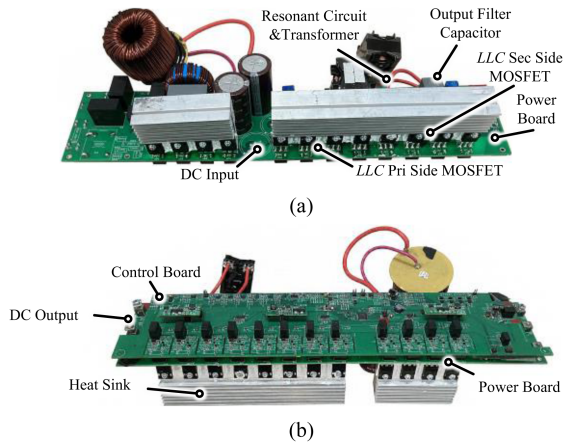

Fig. 14. Hardware prototype. (a) Bottom view of the power board. (b) Top view of the assembled prototype with power board and control board.

FB to HB TPM. As shown in the enlarged view at the TPM moment of SPTMC in Fig. 16, when TPM is performed, the switching frequency suddenly steps to the desired value, which is in conformity with the principle of SPTMC.

Fig. 17 shows the key waveform of the TPM *LLC* converter under SPTMC during TPM due to the sudden change of input voltage and reference output voltage. It can be seen that except for the scenario that the *LLC* converter switches from HB to FB because of the reference output voltage step up in Fig. 17(b), there is almost no oscillation during the TPM. The reason why output voltage overshoot during the reference output voltage step-up is that the SPTMC suddenly change the switching frequency to the desired value of the reference voltage rather than the voltage at the TPM moment.

C. Prototype Efficiency

In Fig. 18, the efficiency of the *LLC* converter in HB and FB modes is presented. It can be seen that the efficiency of the FB

TABLE III
PROTOTYPE SPECIFICATION

Items	Value
Switches Q_1–Q_4	UF3C065040K4S, 52 mΩ @I_D=40 A, T_J=25°C Snubber capacitor: 220 pF Dead time: 200 ns
Diode D_1–D_4	UF3C065040K4S (reverse diode only, without synchronous rectification), 1.5 V @ I_F=20 A, T_J=25°C
Transformer T	Turns ratio: n = 12:10 Magnetizing inductor L_m: 40 μH
Resonant inductor L_r	14.3 μH
Resonant capacitor C_r	7*15 nF in parallel, MLCC, C0G
Output filter capacitor C_o	6*4.7μF in parallel, film capacitor
MCU	SPC58NN84E7

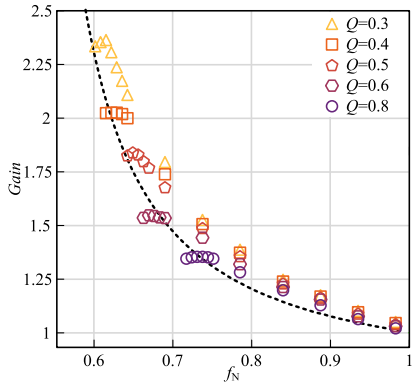

Fig. 15. Peak gain trajectory predicted via geometrically simplified SPA (dashed line) and experimental results.

mode *LLC* converter rapidly drops with the decreasing reference voltage in the buck mode. This is because of the incremental turn-OFF loss of switches and the core loss of both the resonant inductor and transformer due to the rising switching frequency. When the output voltage is lower than 90 V, the efficiency of HB mode is greater than that of FB mode. By switching to HB mode, the efficiency of the *LLC* converter can be improved when the output voltage is lower than 90 V. While the output voltage is higher than 100 V, to maintain high efficiency, the converter will switch to FB mode.

From the perspective of voltage gain, TPM *LLC* also enjoys advantages against the traditional FB *LLC*, as shown in Fig. 18. When the output voltage is 77 V and the switching frequency of FB mode reaches 250 kHz (1.7 times of f_r). However, further increasing the switching frequency may reduce the reliability of the converter. By switching to HB mode, the lower output voltage limit can be easily extended to 50 V.

With the proposed design procedure, the existence of a stable operating point after TPM from FB to HB is guaranteed. In HB mode, the output voltage at $f_{N,\min}$ ($0.6f_r$ = 90 kHz) is 110 V, which is higher than the threshold voltage gain M_{th}, and thus the stability of the *LLC* converter during TPM is ensured.

The power-versus-efficiency curves of FB and HB *LLC* converter with different voltages near the potential TPM region are depicted in Fig. 19. It can be seen that at the FB mode resonance point (100 V), the efficiency of the FB mode is consistently

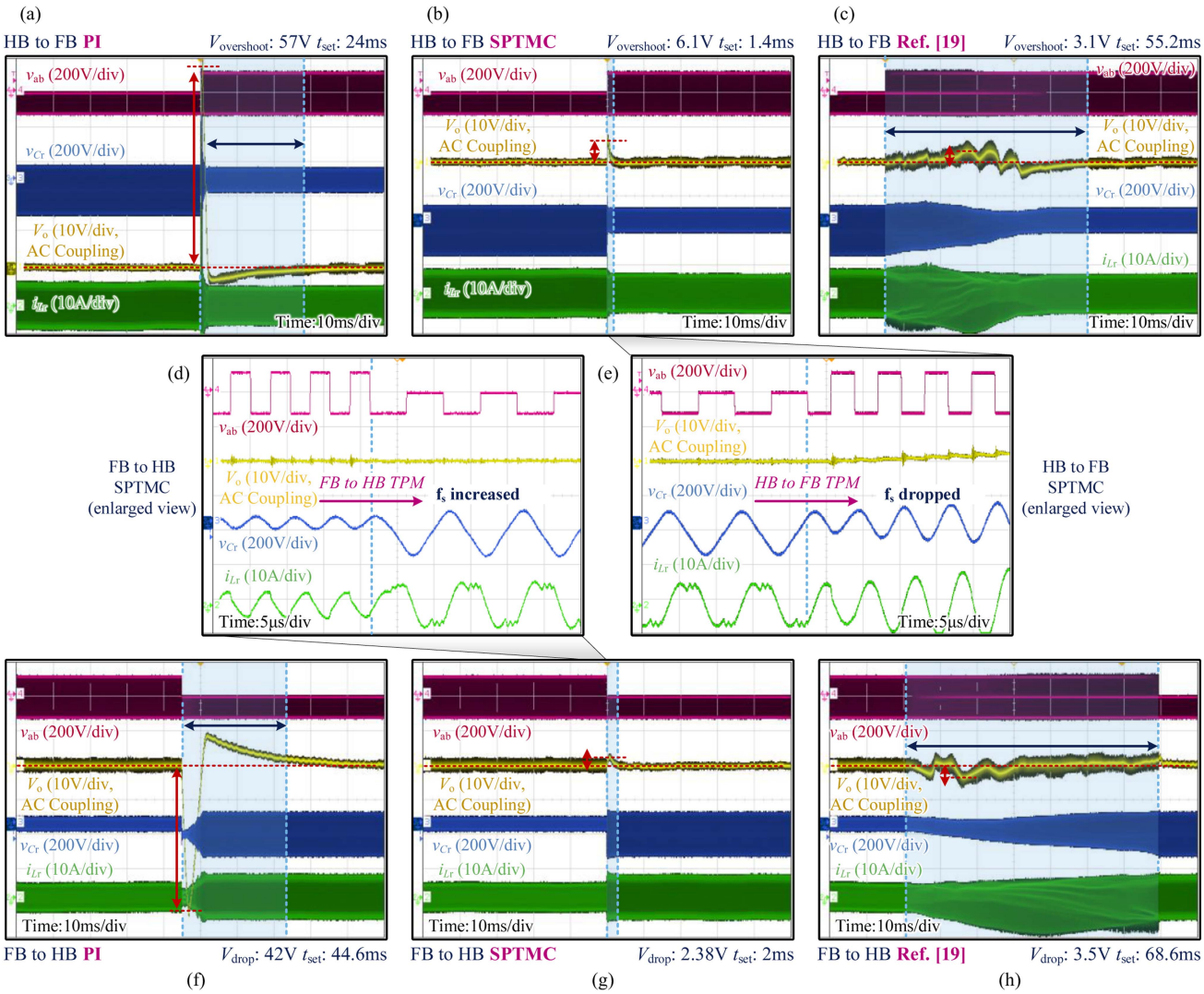

Fig. 16. Key waveform of TPM *LLC* converter switching between FB and HB mode under different controllers, where the blue region refers to the transient process. HB to FB with (a) PI controller only, (b) SPTMC, (c) strategy in [19], and (d) enlarged view of SPTMC. FB to HB with (a) PI controller only, (b) SPTMC, (c) strategy in [19], and (d) enlarged view of SPTMC.

TABLE IV
COMPARISONS OF DIFFERENT SMOOTH TPM CONTROL FOR *LLC* CONVERTER

Items	OTC [22]	OTC [23]	Reference [15]	Reference [19]	Proposed SPTMC
Dynamic performance	FB-HB: 5 cycles HB-FB: 3 cycles	FB-HB: 100 cycles HB-FB: 200 cycles	FB-HB: 100 cycles HB-FB: 200 cycles	More than 2000 cycles for both situations	FB-HB: 100 cycles HB-FB: 200 cycles
Modulation or control mode morphing	OTC during TPM	OTC during TPM	Not needed	PWM during TPM	Not needed
Cycle-by-cycle control	Needed	Needed	Not needed	Not needed	Not needed
Lookup table	Not needed	Needed	Collected though experiment	Not needed	Not needed
Existence of a stable operating point after TPM	Guaranteed	Not guaranteed	Guaranteed during experiment	Not guaranteed	Guaranteed during design procedure
Voltage gain range	Resonant point only	1–4	1–3	1–4	1–4

higher than that of the HB mode. However, when operating in FB buck mode, the FB mode *LLC* converter tends to exhibit lower efficiency compared to the HB mode under light load conditions. When the output voltage is set to 80 V, only the full load point falls within the switching frequency limit.

Different smooth TPM control for *LLC* converter are listed in Table IV. To sum up, the proposed SPTMC features guaranteed stable operating points after TPM and a wide voltage gain range of 1–4 while maintaining a fast dynamic performance. Meanwhile, neither extra modulation, control

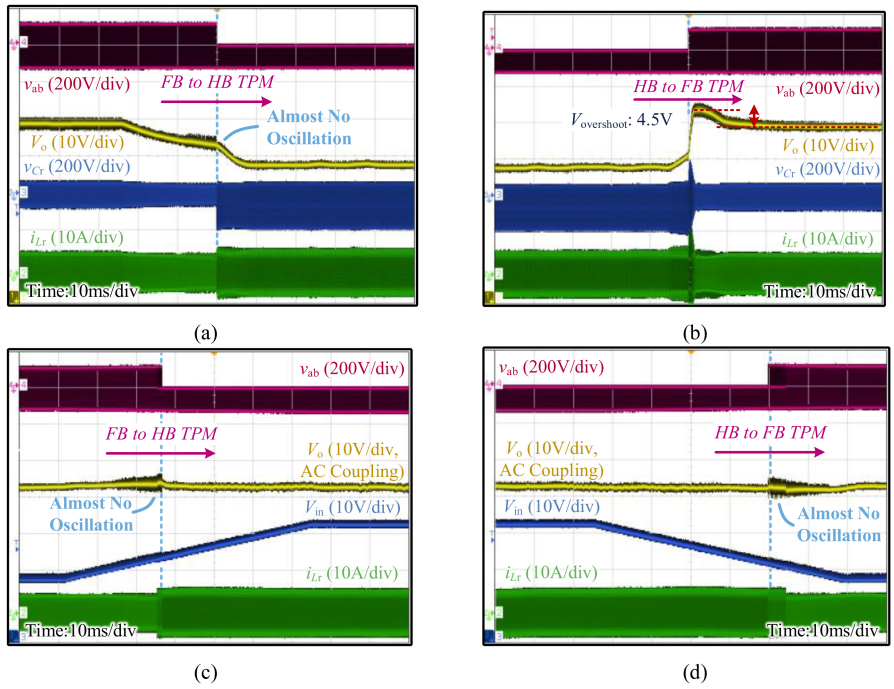

Fig. 17. Key waveform of *LLC* converter with SPTMC during TPM. (a) FB to HB due to reference voltage step down. (b) HB to FB due to reference voltage step-up. (c) FB to HB due to input voltage step up. (d) HB to FB due to input voltage step down.

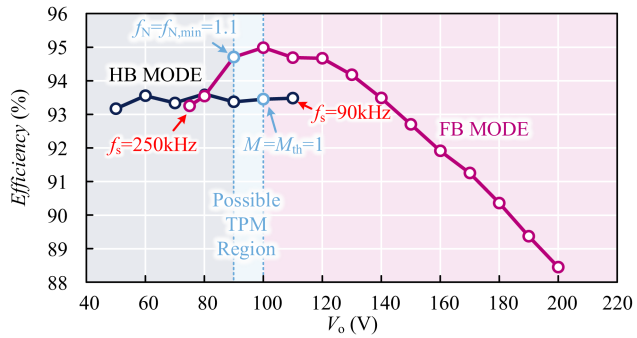

Fig. 18. Efficiency of *LLC* converter for both FB mode (purple line) and HB mode (blue line) at full load when the input voltage is 120 V.

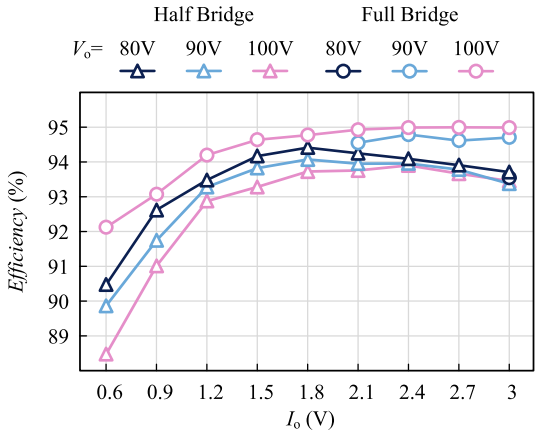

Fig. 19. Power-versus-efficiency curves of FB and HB *LLC* converter with different voltages near the potential TPM region, when the input voltage is 120 V.

mode morphing (except the modulation switching of the morphing leg due to the TPM), cycle-by-cycle control nor a lookup table is required in the SPTMC control, which enhances the control stability and reduces the MCU performance requirements.

VI. Conclusion

In this article, a novel design procedure together with a corresponding seamless topology morphing control has been proposed for FB and HB morphing *LLC* converters. The peak voltage gain trajectory of the *LLC* converter is predicted via geometrically simplified SPA to help the design process and enhance the system's stability. The expression is given and the predicted result shows good accuracy with both the simulation and experimental results. The seamless topology morphing control involves forecasting the desired frequency after topology switching and incorporating it into the conventional linear controller through feedforward control. The implementation is simple and suitable for low-cost MCU applications.

A prototype is built, and the experimental results are presented to validate the feasibility of the proposed design procedure and control scheme. The results demonstrate that the existence of a stable operating point after TPM is guaranteed, leading to improved dynamic performance during topology switching. Moreover, the steady-state characteristics reveal a widened voltage gain range of 1–4 for the *LLC* converter and improved efficiency in low-gain situations.

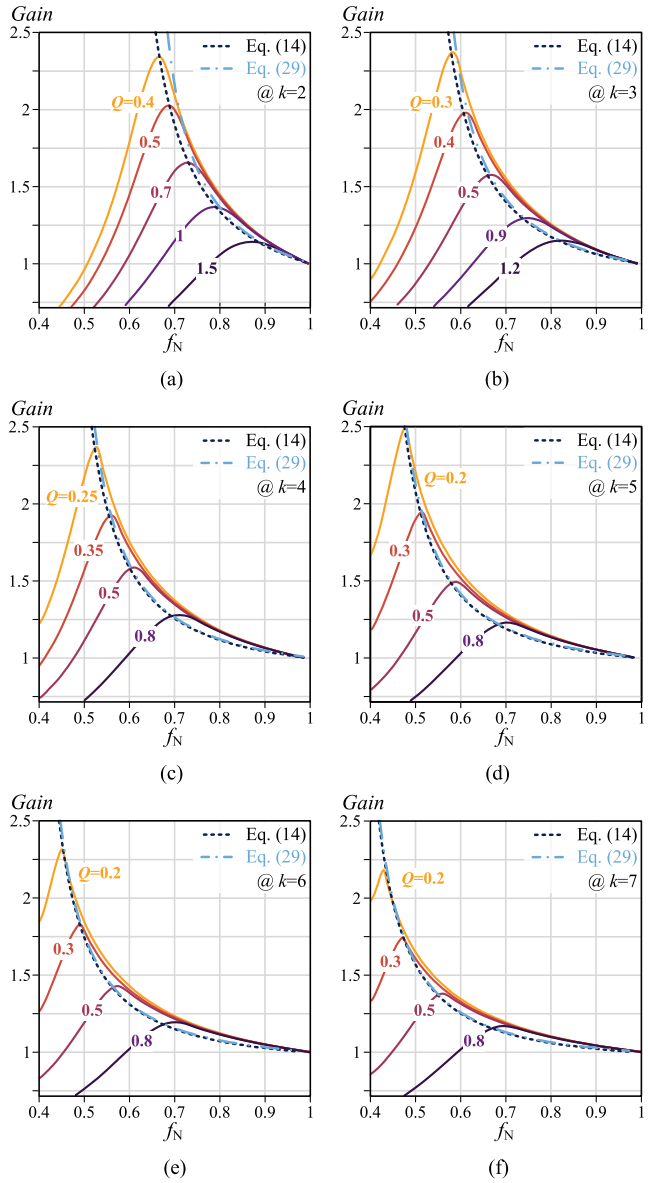

Fig. 20. Comparison of the peak gain trajectory predicted via (14) and (29) and the simulation result. (a) $k = 2$. (b) $k = 3$. (c) $k = 4$. (d) $k = 5$. (e) $k = 6$. (f) $k = 7$.

APPENDIX

According to the derivation, the true expression of $t_{\rm I}$ should be

$$t_{\rm I} = \frac{1}{\omega_{\rm r}} \arcsin \frac{1}{\frac{\sqrt{k+1}}{\sin[\frac{4kf_{\rm N}}{\pi\sqrt{k+1}}(2-\frac{1+a}{nV_{\rm oN}})]} + (\frac{1+a}{nV_{\rm oN}} - 1)\frac{2kf_{\rm N}}{\pi}}. \quad (29)$$

Equation (14) is the result obtained by mistakenly writing the end $V_{\rm in}$ as $V_{\rm o}$ during the first time derivation. However, as shown in Fig. 20, when k is between 2 and 7, the maximum gain curve predicted by (14) enjoys better accuracy with the simulation results than (29). Therefore, (14), which is modified from (29), can more accurately reflect the maximum gain trajectory of the *LLC* converter and is chosen as the expression of $t_{\rm I}$ in this article.

REFERENCES

[1] B. Yang, F. C. Lee, A. J. Zhang, and G. Huang, "LLC resonant converter for front end DC/DC conversion," in *Proc. IEEE 17th Annu. Appl. Power Electron. Conf. Expo.*, 2002, pp. 1108–1112.

[2] B. Lu, W. Liu, Y. Liang, F. C. Lee, and J. D. van Wyk, "Optimal design methodology for LLC resonant converter," in *Proc. IEEE Appl. Power Electron. Conf.*, 2006, pp. 19–23.

[3] L. Kong, Y. Lu, Y. Wang, and X. Li, "Design of LLC resonant converter based on planar transformer," in *Proc. IEEE 12th Energy Convers. Congr. Expo. - Asia*, 2021, pp. 44–49.

[4] H. Wang, S. Dusmez, and A. Khaligh, "Design and analysis of a full-bridge LLC-based PEV charger optimized for wide battery voltage range," *IEEE Trans. Veh. Technol.*, vol. 63, no. 4, pp. 1603–1613, May 2014.

[5] X. Wang, G. Du, M. Wu, Q. Song, and Y. Chen, "Two-step robust design of LLC converter with corner judgment and greedy algorithm," *IEEE Trans. Power Electron.*, vol. 37, no. 6, pp. 6259–6264, Jun. 2022.

[6] M. F. Menke, J. P. Duranti, L. Roggia, F. E. Bisogno, R. V. Tambara, and Á. R. Seidel, "Analysis and design of the LLC LED driver based on State-space representation direct time-domain solution," *IEEE Trans. Power Electron.*, vol. 35, no. 12, pp. 12686–12701, Dec. 2020.

[7] N. Li, Z. Qin, H. Wang, Q. Shi, and Y. Lin, "Charing pile," U.S. Patent 10 926 655, Feb. 23, 2021.

[8] J. Ge, X. Wang, and Y. Lin, "Charging pile system with a plurality of charging piles switchable in series and parallel," U.S. Patent 10 919 403, Feb. 16, 2021.

[9] P. Jia, T. Guo, X. Zhu, and T. Shao, "A control strategy for the Bidirectional LLC-L converter to extend the gain range based on the time domain analytical model," *IEEE Trans. Power Electron.*, vol. 38, no. 4, pp. 4876–4893, Apr. 2023.

[10] Y. Wei, Q. Luo, and A. Mantooth, "Hybrid control strategy for LLC converter with reduced switching frequency range and circulating current for hold-up time operation," *IEEE Trans. Power Electron.*, vol. 36, no. 8, pp. 8600–8606, Aug. 2021.

[11] Z. Li, B. Xue, and H. Wang, "An interleaved secondary-side modulated LLC resonant converter for wide output range applications," *IEEE Trans. Ind. Electron.*, vol. 67, no. 2, pp. 1124–1135, Feb. 2020.

[12] B. Xue, H. Wang, J. Liang, Q. Cao, and Z. Li, "Phase-shift modulated interleaved LLC converter with ultrawide output voltage range," *IEEE Trans. Power Electron.*, vol. 36, no. 1, pp. 493–503, Jun. 2021.

[13] G. Zhu, J. Dong, W. Shi, T. B. Soeiro, J. Xu, and P. Bauer, "A mode-switching-based phase shift control for optimized efficiency and wide ZVS operations in wireless power transfer systems," *IEEE Trans. Power Electron.*, vol. 38, no. 4, pp. 5561–5575, Apr. 2023.

[14] Z. Liang, R. Guo, G. Wang, and A. Huang, "A new wide input range high efficiency photovoltaic inverter," in *Proc. IEEE Energy Convers. Congr. Expos.*, 2010, pp. 2937–2943.

[15] Y. Wei, Q. Luo, and H. Alan Mantooth, "A novel LLC converter with topology morphing control for wide input voltage range application," *IEEE J. Emerg. Sel. Topics Power Electron.*, vol. 10, no. 2, pp. 1563–1574, Apr. 2022.

[16] W. Inam, K. K. Afridi, and D. J. Perreault, "Variable frequency multiplier technique for high-efficiency conversion over a wide operating range," *IEEE J. Emerg. Sel. Topics Power Electron.*, vol. 4, no. 2, pp. 335–343, Jun. 2016.

[17] X. Fang, H. Hu, Z. J. Shen, and I. Batarseh, "Operation mode analysis and peak gain approximation of the LLC resonant converter," *IEEE Trans. Power Electron.*, vol. 27, no. 4, pp. 1985–1995, Apr. 2012.

[18] Y. Wei, Q. Luo, Z. Wang, and H. A. Mantooth, "A complete step-by-step optimal design for LLC resonant converter," *IEEE Trans. Power Electron.*, vol. 36, no. 4, pp. 3674–3691, Apr. 2021.

[19] M. M. Jovanović and B. T. Irving, "On-the-fly topology-morphing control—Efficiency optimization method for LLC resonant converters operating in wide input- and/or output-voltage range," *IEEE Trans. Power Electron.*, vol. 31, no. 3, pp. 2596–2608, Mar. 2016.

[20] W. Feng, F. C. Lee, and P. Mattavelli, "Simplified optimal trajectory control (SOTC) for LLC resonant converters," *IEEE Trans. Power Electron.*, vol. 28, no. 5, pp. 2415–2426, May 2013.

[21] W. Feng and F. C. Lee, "Optimal trajectory control of LLC resonant converters for soft start-up," *IEEE Trans. Power Electron.*, vol. 29, no. 3, pp. 1461–1468, Mar. 2014.

[22] C. Fei, M. H. Ahmed, F. C. Lee, and Q. Li, "Two-stage 48 V-12 V/6 V-1.8 V voltage regulator module with dynamic bus voltage control for light-load efficiency improvement," *IEEE Trans. Power Electron.*, vol. 32, no. 7, pp. 5628–5636, Jul. 2017.

[23] D. Sha and X. Yang, "Wide voltage input full bridge(FB)/half bridge(HB) morphing-based LLC DC–DC converter using numerical optimal trajectory control," *IEEE Trans. Ind. Electron.*, vol. 70, no. 4, pp. 3697–3707, Apr. 2023.
[24] C. Zhang and P. Barbosa, "Modulation transition methods based on trajectory control for *LLC* resonant converters operating in wide input- and/or output-voltage range," *IEEE Trans. Power Electron.*, vol. 37, no. 12, pp. 14103–14114, Dec. 2022.
[25] Y. Wei, T. Pereira, Y. Pan, M. Liserre, F. Blaabjerg, and H. A. Mantooth, "A general and automatic RMS current oriented optimal design tool for LLC resonant converters," *IEEE J. Emerg. Sel. Topics Power Electron.*, vol. 10, no. 6, pp. 7318–7332, Dec. 2022.
[26] U. Kundu, K. Yenduri, and P. Sensarma, "Accurate ZVS analysis for magnetic design and efficiency improvement of full-bridge LLC resonant converter," *IEEE Trans. Power Electron.*, vol. 32, no. 3, pp. 1703–1706, Mar. 2017.

Jie Chen (Student Member, IEEE) was born in Shanghai, China, in 1998. He received the B.S. degree in electrical engineering from Shanghai Jiao Tong University, Shanghai, China, where he is currently working toward the Ph.D. degree in electrical engineering.

His research interests include wide bandgap devices, *LLC* converters, and wireless power transfer.

Junzhong Xu (Member, IEEE) was born in Ningbo, China, in 1994. He received the B.S. degree in electrical engineering from the Harbin Institute of Technology, Harbin, China, in 2016, and the Ph.D. degree in electrical engineering from Shanghai Jiao Tong University, Shanghai, China, in 2021.

From 2020 to 2021, he was a visiting scholar with the dc Systems, Energy Conversion and Storage Group, Delft University of Technology, Delft, The Netherlands. He was a Postdoctoral Research Fellow with the Department of Electrical Engineering, Shanghai Jiao Tong University, in 2021. He is currently with Power Electronic Systems Laboratory, Swiss Federal Institute of Technology (ETH), Zurich, Switzerland. His research interests include advanced control and modulation for power converters.

Dr. Xu was the recipient of the Outstanding Ph.D. Thesis Award from Shanghai Jiao Tong University in 2021.

Yong Wang (Member, IEEE) received the Ph.D. degree in power electronics from Zhejiang University, Hangzhou, China, in 2005.

From 2005 to 2008, he was a Senior Researcher with Samsung Advanced Institute of Technology, Yongin City, South Korea, working on the fuel cell grid-tied inverters. From 2008 to 2010, he was with Danfoss Solar Inverters, Soenderborg, Denmark, as a Power Electronics Hardware Engineer. In 2010, he joined Shanghai Jiao Tong University, Shanghai, China, where he is currently a Full Professor with the Department of Electrical Engineering. His research interests include new energy storage systems and electric vehicle power supply systems.